Halogenated Terephthalic Acid "Antenna Effects" in Lanthanide-SURMOF Thin Films

Jaciara C. C. Santos,* Yohanes Pramudya, Marjan Krstić, Dong-Hui Chen, Beatrice Lilli Neumeier, Claus Feldmann, Wolfgang Wenzel, and Engelbert Redel

ABSTRACT: Lanthanide based crystalline coatings have a great potential for energy conversion devices, but until now luminescent surface anchored materials were difficult to fabricate. Thin films, called lanthanides surface mounted metal−organic frameworks (SURMOFs) with tetrasubstituted halide (fluorine, chlorine, and bromine) terephthalic acid derivative linkers as a basic platform for optical devices, exhibit a high quantum yield of fluorescence visible to the naked eyes under ambient light. We show that we can tune the luminescent properties in thin films by halide substitution, which affords control over the molecular structure of the material. We rationalize the mechanism for the modulation of the photophysical properties by "antenna effect", which controls the energy transfer and quantum yields using experimental and theoretical techniques for chelated lanthanides as a function of the type of atom substitutions at the phenyl rings and the resulting dihedral angle between phenyl rings in the linkers and carboxylate groups.

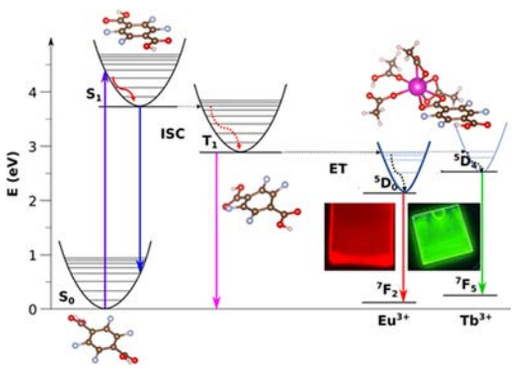

KEYWORDS: *lanthanides, MOF, fluorescence, halogenated, terephthalic acid, antenna effect*

INTRODUCTION

Luminescent lanthanide ions have attracted scientific and technological interests due to their unique photophysical and magnetic properties and applications in the fields of optics, photonics, and biomedicine, security inks, lasers, and magnetic resonance imaging.[1,2] Their unique luminescent properties, such as characteristic sharp emissions in the near IR and visible spectral regions, long lifetime, large Stokes shifts, and high color purity, can be combined with the structural properties of metal−organic frameworks (MOFs). MOF is a class of porous materials comprised of coordination bonds between metal nodes or secondary building units (SBUs) and organic linkers to form nets or frameworks. The nets are extended along two dimensional (2D) or three dimensional (3D) chains, resulting in a crystalline open framework with permanent porosity. There is a large amount of available linker molecules and inorganic building blocks for synthesizing MOFs, resulting in an estimated number of about 70 000 different MOF types developed so far,[3] most of them in the form of powders. The formation and processing of MOF thin films, also called lanthanides surface mounted metal−organic frameworks (SURMOFs), are required in advanced technological applications, such as optical coatings and optoelectronic devices.[4] Despite a multitude of potential applications of lanthanide MOFs (Ln MOFs), real devices are still missing.[5,6]

Although there are many methods for producing thin film MOFs, one of the most appealing procedures is the layer by layer (LbL) assembly deposition because it offers an easy and inexpensive way to produce high yield films with precise composition control in relatively fast processes. The LbL approach involves the sequential deposition of two or more materials that can be held together physically or chemically. This sequential deposition can take distinct routes of assembly, such as immersive, spin, spray, or electromagnetic as well as fluidic deposition (see Figure 1). The growth of MOF thin films using this approach was first demonstrated by Shekhah et al.[7] In the immersive LbL process, the thin films were prepared by sequentially dipping a chemically functionalized substrate into the solutions of the different building units. Between steps, the substrate was rinsed with the solvent to remove the unreacted or weakly physisorbed reactants. In optimal conditions, the number of deposition cycles determined the final thickness of the thin films.

SURMOFs were rarely reported with Ln^{III} ions as the metal nodes (SBU) using a LbL approach. To the best of our knowledge, only two LbL assisted Ln SURMOFs were

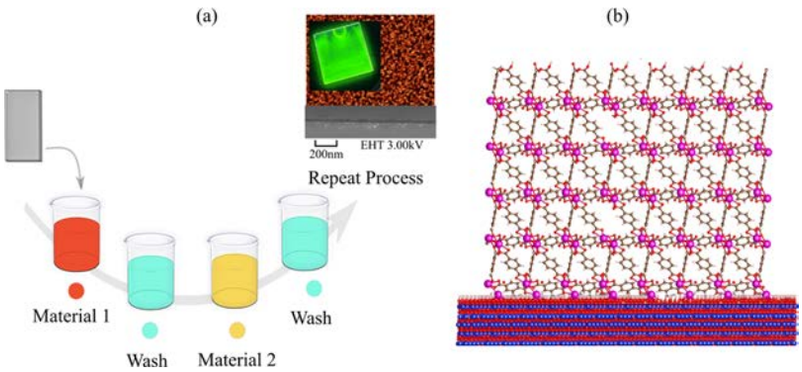

Figure 1. (a) Illustration of the LbL immersive route to produce homogeneous thin films and (b) the SURMOFs on top of silicon substrate after several cycles.

reported so far: MOF 76[8] and Eu NDC.[9] Ln SURMOFs are mainly prepared with the following methods:

(1) solvothermal deposition,[10] where a functionalized surface is exposed to a solution containing the mixture of the MOF synthesis precursors (this process can be electrochemically[11] or microwave assisted[12]) and

(2) postsynthesized Ln MOF suspension, which can be directly spin coated[13] or electrophoretically[14] deposited on a surface; alternatively, Ln^{III} can also be loaded inside the pores of prefabricated SURMOFs.[15]

Tuning luminescent properties in thin films require mastery over the molecular structure, and conformation of how the organic molecules are packed together, including an understanding of how their behavior changes when they get excited, e.g., by UV light or other external stimuli.[16] Unlike conventional amorphous LbL thin films, SURMOF formation adds control over the conformation of the building block molecules because they crystallize and can be grown in an oriented way on a prefunctionalized substrate. The choice of the building blocks for the SURMOFs allows the design of responsive and functional MOF thin films for various advanced technological applications. Due to their photophysical properties, lanthanide ions are ideal luminescent centers for SURMOFs. The shielding of the 4f valence orbitals and the variety of electronic levels generated by the 4f electronic configurations make trivalent lanthanide based materials promising candidates for the preparation of wavelength converting devices and sensitive probes. However, the selection of suitable organic linkers has to be considered with regard to the known "antenna effect".[17−20] Here, terephthalate as a sensitizer chromophore is used as a light harvesting antenna and subsequent excited state energy transfer generates the emitting lanthanide centered excited state. Since Ln trivalent cations (Ln^{III}) themselves exhibit very low absorption and emission probabilities, they need a strongly absorbing ligand for energy transfer via antenna effect. Terephthalic acid (t H BDC) and its derivatives (R BDC) have been reported as successful linkers for numerous lanthanide MOF synthesis.[21−23] Tetrafluoroterephthalic acid (t F BDC) is a remarkable and versatile ligand for the construction of new coordination polymers and metal−organic frameworks.[21−24] It has been reported as a linker for MOF single crystal synthesis with most of the trivalent lanthanides. Only MOFs with the La^{III} and Lu^{III}, the largest and the smallest lanthanide cations, as well as with the radioactive Pm^{III}, are still unknown.[24] In addition, it is already known that MOFs with perfluorinated linkers give rise to strong emission because the quenching due to C−H related vibronic states is strongly reduced.[25]

Recently, Smith et al.[26] reported the synthesis of Ln MOFs using tetrabromoterephthalic acid (t Br BDC) with most of the trivalent lanthanides ions. The authors reported two series of MOF structures and demonstrated for the first time that the decrease in the lanthanide ions size results in a change in the structure from a two dimensional (2D) MOF to a three dimensional (3D) MOF. Ln MOFs with tetrachlorinated BDC (t Cl BDC) ligands have so far been reported with only La^{III} ion[27] forming five new structures by changing its crystallizing medium. In a comparative study, the authors observed that, although the ligand and the metal choices are very important for the MOF design, the size of the carbonyl solvent molecules in the synthesis also plays a determining rule, affecting the coordination geometries around the La^{III} ions, the coordination modes of carboxylate groups, the packing arrangements, and the void volumes of the overall crystal lattices.

Compared to the transition metals more commonly applied for MOF synthesis, the design of Ln MOFs is more complex due to the high and variable coordination numbers (CN) of the trivalent lanthanide ions. On the other hand, the flexible coordination geometry hampers the prediction and control of the synthesized Ln MOF structures; however, on the other hand, it opens the option to synthesize unusual and new architectures.[28−31] With the same lanthanide and organic linker, it is possible to realize distinct crystal structures.[23] Since the pioneering synthesis by Reineke et al.,[32] Ln MOF syntheses with BDC and derivatives reported structures crystallizing mostly in monoclinic and triclinic space groups. Orthorhombic[33−35] and cubic[36] space groups were rarely reported.

The BDC molecule and its halogenated derivatives have distinct geometries. The dihedral angle between the benzene ring and the COOH plane is nearly 90° for Cl and Br substitutes, whereas these planes are nearly parallel for F and H. Here, we investigate the correlation between the atom substitution in the BDC structure with the photoluminescent, the energy transfer, quantum yield results, and structural properties of the resulting Ln SURMOFs.

RESULTS AND DISCUSSION

Luminescent SURMOFs with Tb^{III} and Eu^{III} were successfully prepared using the dip coating LbL method with the halogen tetrasubstituted terephthalic ligands. We studied the organic linkers: tetrafluoroterephthalic (t F BDC), tetrachlorotereph

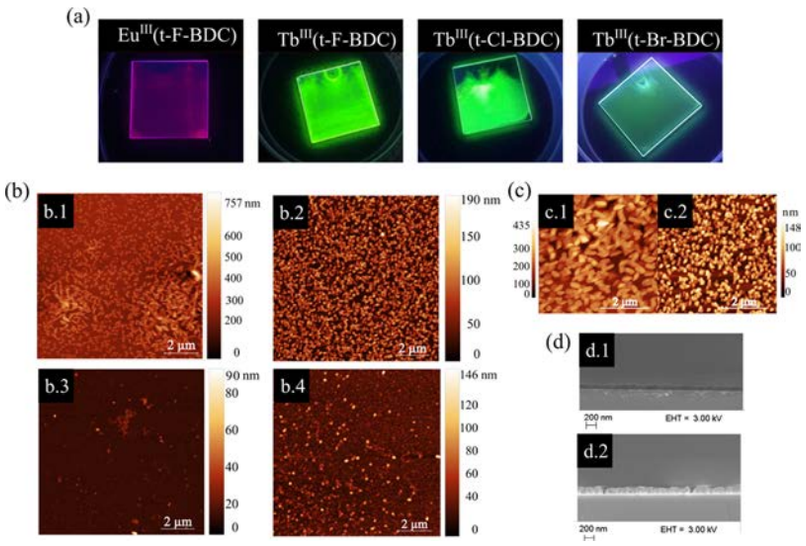

Figure 2. (a) Thin films prepared on fused quartz substrates (1.5 × 1.5 cm^2) under UV radiation (254 nm): Eu^{III}(t F BDC), Tb^{III}(t F BDC), and Tb^{III}(t Cl BDC) with 45 cycles and Tb^{III}(t Br BDC) with 90 cycles. (b) Atomic force microscopy (AFM) topology (10 μm × 10 μm) of 1 Eu^{III}(t F BDC) and 2 Tb^{III}(t F BDC) thin films with 45 cycles, and 3 Tb^{III}(t Cl BDC) and 4 Tb^{III}(t Br BDC) with 80 and 90 cycles, respectively. (c, d) AFM topology (5 μm × 5 μm) of Eu^{III}(t F BDC) and Tb^{III}(t F BDC) on Si substrates with 45 cycles and their respective cross sectional scanning electron microscopy (SEM) images.

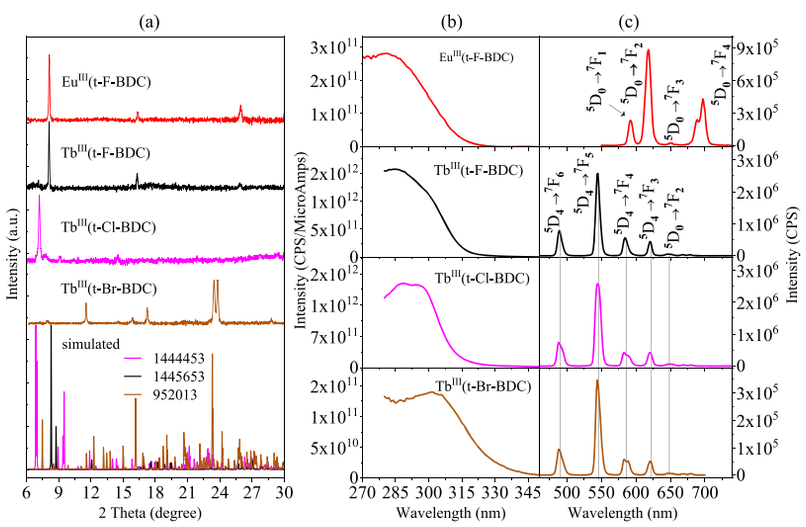

Figure 3. Out of plane XRD and PL measurement data for the thin films. (a) Out of plane XRD data of thin films on silicon substrates of Eu^{III}(t F BDC), Tb^{III}(t F BDC), prepared with 45 cycles, and Tb^{III}(t Cl BDC) and Tb^{III}(t Br BDC) with 90 and 85 cycles, respectively, and simulated XRD pattern for the structures with CCDC nos. 1868639, 1444453, and 1445653. (b) Excitation and (c) emission spectra for the respective thin films (1−3) with 45 cycles and (4) with 85 cycles prepared on fused quartz substrates.

thalic (t Cl BDC), and tetrabromoterephthalic (t Br BDC) acid. SURMOF growth with Eu^{III} was only observed with the t F BDC ligand. SURMOFs with the t F BDC linker, i.e., Tb^{III}(t F BDC) and Eu^{III}(t F BDC), can be prepared at room temperature. In contrast, SURMOFs with t Cl BDC and t Br BDC were prepared at an elevated temperature of 60 °C. Tb^{III}(t F BDC) and Eu^{III}(t F BDC) prepared at room temperature are inhomogeneous and easily detached from the quartz surface. Moreover, we observed large areas with strong luminescence as well as totally uncovered areas. This limitation could be tackled by two measures: (i) increasing the temperature and (ii) adding MF to the organic linker solution. A small rate of 1.35% of dimethylformamide (DMF) turned out to be sufficient to obtain a good surface coverage. Eu^{III} SURMOFs with t Cl BDC and t Br BDC were not observed either at room temperature or at 60 °C. The BDC ligand without halogen substitution was also investigated under distinct LbL approaches, but no luminescent crystalline thin films were observed. See the Supporting Information for more details.

Figure 2a compares Eu^{III}(t F BDC), Tb^{III}(t F BDC), Tb^{III}(t Cl BDC), and Tb^{III}(t Br BDC) thin films under UV radiation (254 nm) prepared on quartz substrates and its SPM topologies characterization on Si surfaces.

AFM topology characterizations from both Tb^{III}(t F BDC) and Eu^{III}(t F BDC) exhibit similar slightly elongated crystal shapes covering Si surface (see Figure 2b.1,b.2,c.1,c.2). The cross sectional SEM images also exhibited stacked elongated crystals (Figure 2d.1,d.2). We observe Eu^{III}(t F BDC) crystals of about 100 nm in height and Tb^{III}(t F BDC) crystals with a

height of nearly 200 nm. The thin films prepared with Tb^{III}(t Cl BDC) and Tb^{III}(t Br BDC) are luminescent but often remain amorphous (see Figure 2b.3,b.4).

In addition, Figure 3a shows the out of plane X ray diffraction (XRD) data for Tb^{III}(t F BDC), Eu^{III}(t F BDC), Tb^{III}(t Cl BDC), and Tb^{III}(t Br BDC) on Si substrates. Tb^{III}(t F BDC) and Eu^{III}(t F BDC) SURMOFs prepared with only 45 cycles exhibit strong luminescence and crystallinity. Only after a minimum of 90 deposition cycles, weak XRD peaks could be observed, although often the surface consists of amorphous thin films, which was also found by the AFM topology analysis.

A series of Ln MOFs structures were reported with these building blocks by regulating solvents where the distinct configuration of the metal center can be achieved, or by changing the ion size (La−Lu), as demonstrated for t Cl BDC and t Br BDC ligands, respectively.[26,27] A comparative analysis is difficult since most Ln MOFs syntheses mix a variety of solvents at different ratios. Here, we selected results obtained under mild laboratory conditions and alcohol based main crystallizing medium (ethanol or methanol) to search for structures closer to those using the LbL process. In Figure 3a, the thin film's XRD data is compared to the simulated XRD pattern for the selected Ln MOFs with t Br BDC, t Cl BDC, and t F BDC (CCDC 1868639, 1444453, and 1445653). Most Ln MOFs with t Br BDC ligand crystallize into a triclinic space group with an eight coordinated coordination environment when synthesized under mild condition, whether the crystallizing media was only water (CCDC 1868639) or ethanol (CCDC 952013).[26,37] In an alcohol based solvent, the triclinic group symmetry is also preferred for the t Cl BDC ligand (with additional carbonyl molecules such as DMF, diethylformamide (DEF), etc.).[26,37] For the t F BDC ligand, a monoclinic system is preferred for this crystallization medium.[22,24,38]

The thin films seemed to grow in preferred orientations because the number of peaks observed in the out of plane XRD was reduced, giving rise to a structure assignment difficulty. Eu^{III}(t F BDC) and Tb^{III}(t F BDC) seemed to be isostructural, but Tb^{III}(t Cl BDC) and Tb^{III}(t Br BDC) exhibited rather different XRD patterns.

Excitation and emission spectra of Tb^{III}(t F BDC), Eu^{III}(t F BDC), Tb^{III}(t Cl BDC), and Tb^{III}(t Br BDC) thin films on fused quartz substrates are shown in Figure 3b,3c. The thin films with the t F BDC linker exhibit higher emission intensities than the samples with the respective t Cl BDC and t Br BDC ligands. Thin films were prepared with 45 cycles, except for Tb^{III}(t Br BDC), for which the luminescence effects have a rather weak intensity and needed about twice more cycles so the luminescence effects could be monitored. Tb^{III}(t F BDC), Tb^{III}(t Cl BDC), and Tb^{III}(t Br BDC) exhibit the characteristic narrow emission lines transitions of Tb^{III} arising from the $^5D_4$ state to the ^7F_J (J = 6−3) levels. Eu^{III}(t F BDC) similarly exhibits the characteristic narrow emission lines of Eu^{III} arising from the $^5D_0$ state to the ^7F_J (J = 1−4) levels (see also Figure 3c). Tb^{III}(t F BDC) and Tb^{III}(t Cl BDC) SURMOFs exhibit significantly stronger emission intensity than the other halogen SURMOFs.

We investigated the photoluminescent quantum yield (QY), defined as the ratio of the number of emitted photons and the number of absorbed photons. Although there are numerous Ln MOFs reported so far, most publications did not report QY at all. Some of the reported QY values for Ln MOFs synthesized with the t F BDC linker and the metals Eu^{III} and Tb^{III} are summarized in Table 1. Tb^{III} compounds usually exhibit higher luminescence efficiency than Eu^{III} compounds, while the QY values reported for Eu^{III} compounds are more variable. Ln MOFs can be synthesized under rather mild conditions, and small changes in the synthesis route can result in different structures.[38−41] The precise prediction and control of Ln MOFs is challenging due to its high and variable coordination number (CN). For the QY measurements (the QY values are presented in Table 1), the syntheses of luminescent powders were assisted by a simple sonochemical method. The synthesizes were performed under mild conditions at 60 °C in aqueous NaOH (25 mM in a mixture of ethanol and water in a 3:1 ratio). The detailed synthesis description can be found in the Supporting Information.

Table 1. QY Values for Ln(III) Compounds with t F BDC Linker and the Metals Tb^{III} and Eu^{III}

Eu^{III} MOF overall QY (%)	Tb^{III} MOF overall QY (%)	reference
53	67	Sobieray et al.[24]
9	42	Mikhalyova et al.[48]
13	66	this work

Tb^{III}(t F BDC) powders prepared by a sonochemical method achieved 66% QY, which is close to values reported by Sobieray et al.[24] The preparation of powder samples for Tb^{III}(t Cl BDC) and Tb^{III}(t Br BDC) turned out to be more difficult, and QYs could not be reliably determined. Details can be found in the Supporting Information.

THEORY AND MODELING

To elucidate the antenna effect as a function of the halogen atom substitution in the BDC ligand molecules, we investigated the correlation between atom substitution and the QY of the lanthanide SURMOFs with electronic structure calculations. Such a substitution of atoms induces a change of the dihedral angle of the phenyl rings within the BDC linkers relative to the COO plane coordinated to the lanthanide cations as illustrated in Figure 4. These geometrical features are due to the imposed steric effects in the sizes of the atoms (H, F, Cl, Br). For further details, see also Figure S6 and the theory part in the Supporting Information.

We used a molecular cluster model to study the excited states of the systems shown in Figure 4. It consists of one center Eu^{III} cation surrounded by four acetate groups and a BDC linker. This smallest molecular model represented the full crystalline structures of the synthesized SURMOFs. The use of simplified structures with only one BDC linker effectively reduced the complexity of the systems and allowed us to efficiently study the effect of hydrogen substitution in the phenyl ring with halogen atoms and estimated the QY. The relaxed structures of BDC with H and F functionalized phenyl rings have almost flat dihedral angles (Figure 4a), whereas replacing them with Cl and Br caused a rotation of the phenyl ring to an almost perpendicular position relative to the COOH plane, see Figure 4b. The large dihedral angles in Cl and Br BDC compounds hindered the crystallization of the structures in SURMOF growth as described in the Experimental Section (Figure 3). To study the effect of the dihedral angle alone, we calculated the QY of each halide with different dihedral angles

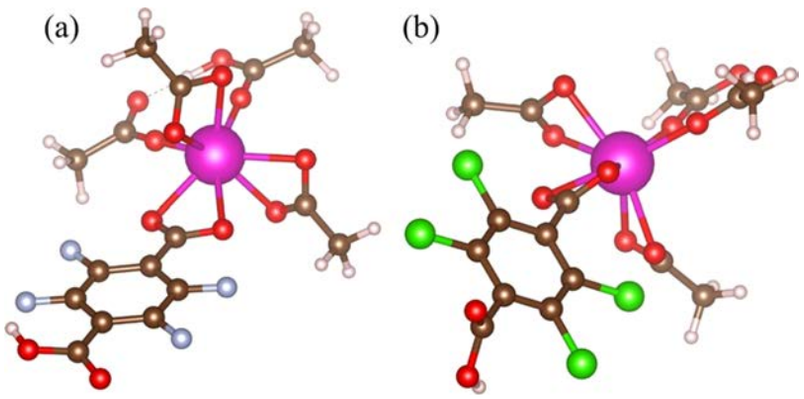

Figure 4. Geometrically optimized molecular model of the Eu complex. Eu (purple), O (red), C (brown), F (gray), Cl (green), and H (white). (a) H and F−BDC dihedral angles between the COO plane with the phenyl ring plane in the BDC linkers are 4−6°. (b) Dihedral angles between the COO and the phenyl ring planes with Cl and Br BDC linker are 80−85°.

between the phenyl group and COO group connected to the Eu^{III} cation (see Figure S6).

First, we described the process of the antenna effects (Jablonski diagram) of the linkers to lanthanides ions, with their corresponding energy levels (eV) shown in Scheme 1. For the ligands (F substituted BDC) alone, we calculated the energy level using the density functional theory (DFT) level.

Scheme 1. Jablonski Diagram of the Ligands and Lanthanides Atoms in the Complex[a]

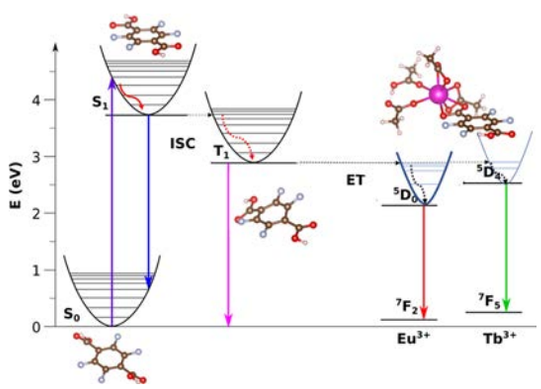

[a]Lanthanides ion Eu^{III} (purple), O (red), C (brown), F (gray), and H (white).

On the abscissa of Scheme 1 are the states of a fluorinated BCD linker and europium complex, and the ordinate is the energy level for each state. Under irradiation by UV light, a singlet excitation is localized on an antenna BDC ligand from S_o to a singlet excited state (upright violet arrow line). The commensurate between the experimental absorption and excitation spectra of lanthanide complexes with the corre sponding spectra of the individual ligands suggests that the lowest excited states are localized on individual ligands, instead of being delocalized over the lanthanide complex.[42,43] Fast nonradiative relaxation from internal conversion subsequently brings the linker to the lowest singlet states S_1 (wiggle red arrow line). From the S_1 excited state geometry, the linker can be deactivated by internal conversion, fluorescence, or intersystem crossing (ISC) to the closest triplet excited states. Nonradiative fast relaxation is followed from any triplet excited states to the local minimum of the lowest triplet states T_1 (wiggle red dashed line).[44,45] From local minima of triplet excited state T_1, energy transfer from the linkers to lanthanides (Eu^{III} and Tb^{III}) proceeds nonradiatively (black dash arrow lines).[42,43,46−48] Finally, lanthanides ions are relaxed to the lowest radiative levels: $^5D_0$ for Eu^{III} and $^5D_4$ for Tb^{III} (wiggle black dashed lines).[49−51]

To investigate the effect of H substitution by halogen atoms and dihedral angles of COO to the phenyl ring plane, we used semiempirical methods integrated into LUMPAC (lanthanide luminescence software package) using the RM1 Sparkle Model[52] implemented in MOPAC for geometry optimization. This was followed by singlet and triplet excited state energy calculations for the lanthanide complexes with INDO/S CIS approach in ORCA.[53−55] The values of these excited states agree with our TD DFT results for the linkers. However, the LUMPAC workflow is only limited to a single Europium compound. By simplifying the theoretical model, we expected the QY to mainly depend on the dihedral angle and the type of atom at the phenyl rings.

First, we estimated the initial values of the Judd−Ofelt intensity parameters (Ω_2, Ω_4, Ω_6)[56,57] of our systems from the extracted values of the emission spectra in Figure 5 for Eu^{III} compounds. We used these parameters as an initial prediction of the semiempirical Judd−Ofelt intensity parameters and

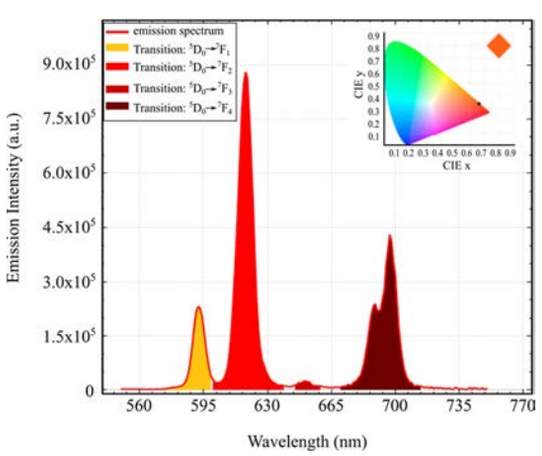

Figure 5. Experimental intensity parameters calculations for Eu^{III}(t F BDC) compounds. The initial experimental Judd−Ofelt Intensity parameters $\Omega_2 = 8.44 \times 10^{-20}$ cm^2 and $\Omega_4 = 11.48 \times 10^{-20}$ cm^2 are calculated based on the typical lifetime of 0.5 ms and refractive index of 1.5. The insert shows the emission color of the compound.

Table 2. Table of Fluorescence Properties[a]

atom type	H	F	Cl	Br
energy state				
RL singlet	6.4767	4.6032	3.5803	4.2376
RL triplet	5.5437	3.6662	3.6752	4.2614
singlet E	36 270.1	33 093.1	37 012.9	36 950.1
triplet E	22 180.3	20 954.5	22 358.8	24 342.9
energy-transfer rate (s^{-1})				
WetMM (singlet → $^5D_4$)	1.88×10^1	1.03×10^4	9.56×10^3	1.37×10^3
WetEX (triplet → $^5D_1$)	3.89×10^2	3.96×10^5	5.86×10^5	1.35×10^4
WetEX (triplet → $^5D_0$)	2.99×10^2	4.03×10^5	4.33×10^5	6.34×10^3
energy back-transfer rates (s^{-1})				
WetMM (singlet → $^5D_4$)	1.54×10^{-17}	3.56×10^{-8}	2.22×10^{-16}	4.28×10^{-17}
WetEX (triplet → $^5D_1$)	1.05×10^{-4}	3.89×10^1	6.74×10^{-2}	1.14×10^{-7}
WetEX (triplet → $^5D_0$)	1.98×10^{-8}	9.68×10^{-3}	1.22×10^{-5}	1.31×10^{-11}
arad (s^{-1})	463.07	463.07	463.77	473.94
anrad (s^{-1})	1532.45	1536.9	1536.23	1526.06
quantum efficiency (%)	23.38	23.15	23.19	23.7
quantum yield (%)	0.16	21.81	20.91	3.88

[a]Details of the quantum yield calculations. RL is the distance between the donor and acceptor, WetMM (s^{-1}) is the energy transfer/back transfer through electric multipole mechanism, and WetEX (s^{-1}) is the energy transfer through an exchange mechanism. Arad is the radiative rate, and anrad is the nonradiative rate.

calculated the energy transfer, back transfer rates, quantum efficiency, and overall QY of the Ln complexes (Table 2).[58] In this calculation, we used the emission lifetime of typical Eu BDC compounds of 0.5 ms. The energy transfer rate was dominated by singlet excited state energy transfer from the ligand to $^5D_4$ excited state of Eu^{III} cation via electromagnetic multipolar mechanism (WetMM) and the triplet state of the ligand to $^5D_0$ and $^5D_1$ via an exchange mechanism (WetEX). The details were tabulated in Table 2.

The theoretically predicted QY of the compounds are compared in Table 3. Simulated QY values are much lower

Table 3. Calculated QY for Eu^{III} Compounds with BDC and Its Halogen Derivatives

compound	quantum yield (QY) [%]	atomic mass	ground state dihedral angle (°)
Eu^{III}(t-H-BDC)	0.2 6.0	1	5
Eu^{III}(t-F-BDC)	19 21	19	5
Eu^{III}(t-Cl-BDC)	13 21	35	72
Eu^{III}(t-Br-BDC)	0.4 3.9	79	84

than the experimentally observed values of crystalline compounds since our model only included the effect of a single Europium atom and a single BDC linker, and replaced the rest of the coordination of BDC linkers with acetates. With this setup, we could focus on the effect of halogenation and dihedral angles of a single BDC linker coordinated to an Eu^{III} ion. We reported the QY as ranges in Table 3 because we explored the effect of dihedral angle changes to the quantum yield by fixing the Eu and acetate molecules and COO plane next to the Eu atom as the phenyl ring in the BDC linker was rotated in the angle range of 0−180°. We found that the dihedral angle did not affect the QYs significantly. The illustration is shown in Figure S6.

The estimated QY is not correlated directly to the dihedral angle; instead, only the type of atom replacing the H results in a large QY gain. The substitution of H atoms with F was predicted to result in the highest average quantum yields, and this agreed with the experimental finding.

We also predicted that the Cl compound may have relatively high QY, which was observed for Tb thin films. We could not test it directly for Eu due to the difficulties of synthesizing Cl compound with Eu in both powder and thin film forms. We note that in Tb based MOF, our experiment showed 6 times higher luminescence intensity in Cl compound than that in Br compound (Figure 3c). The Br thin film preparation needed about twice more deposition cycles (45 vs 85) than Cl thin films and yet Br thin films exhibited luminescence intensity peaks of nearly 1 order of magnitude weaker than the Cl thin films.

CONCLUSIONS

In this manuscript, the fabrication of luminescent Ln SURMOFs thin films with halogen tetrasubstituted tereph thalic acid ligands using an immersive layer by layer method in a short production time is presented. We studied fluorine, chlorine, and bromine terephthalic acid derivatives as building blocks for new Ln SURMOF thin films. The change in the lateral substitutes for the BDC linker, which sterically induces different dihedral angles, shows drastic effects in both measured and calculated QY and affects the Ln SURMOFs photophysical and structural properties. Calculations show that the QY is not correlated directly with the dihedral angle, but with the electronic structure of the complex substituting hydrogens. At the same time, halogen substitution has an effect on the thin film structural conformation, which correlates with the dihedral angles, i.e., it is only possible to synthesize crystalline thin films with halogen substitution. With F substitution, isostructural crystalline coatings with Eu and Tb were obtained; however, for Cl and Br compounds, coatings with poor crystallinity exhibited rather distinct XRD patterns. Fluorine and chlorine linker based thin films exhibited strong luminescence, whereas thin films within the bromine linker had significantly suppressed luminescence. This phenomenon agrees with the theoretical QY calculation. SURMOFs with fluorine linkers could be synthesized at room temperature and exhibit high crystallinity, whereas the luminescent thin films with chlorine and bromine linkers could only be prepared at an

elevated temperature of 60 °C but still show poor crystallinity. The construction of Ln SURMOFs is a versatile platform, not only due to their structural diversity and access to its unique photophysical properties but also because they enable different coordination symmetries of lanthanide centers.

EXPERIMENTAL SECTION

Europium(III) nitrate hexahydrate (99.9%) and terbium(III) trifluoromethanesulfonate (98%) were obtained from Across Organics and Alfa Aeser, respectively. Tetrabromoterephthalic acid and tetrafluoroterephthalic acid (97%) were obtained from Sigma Aldrich. Tetrachloroterephthalic acid (95%) was obtained from abcr. The reagents were used without any further purification. Ethanol (absolute AnalaR NORMAPUR from VWR), fused quartz, microscopy glass slides, and the Si(100) wafers (with a 2 nm native layer of SiO_2) were used as substrates for the thin film growth.

SURMOF Preparation. The thin films were prepared using an automatic LbL coating system (SILAR CONTROLLER, Model No. HO TH 03). The metal and organic linker solutions were prepared in ethanol with concentrations of 0.35 and 0.15 mM, respectively. The immersion times were 30 s in the metal, 5 s for the organic linkers. A rinsing step of 3 s in pure ethanol was added before immersion in each solution to prevent cross contamination between solutions. Additionally, an idle time of 10 s was added after each immersion step.

Substrate Preparation. The Si wafers with a native oxide layer were first cleaned and activated with ozone radiation for 30 min. The SURMOF growth started immediately after this cleaning procedure. The glass substrates were cleaned with KOH solution and then activated with ozone radiation before the SURMOF growth.

X-ray Diffraction (XRD). The out of plane (co planar orienta tion) XRD measurements were collected on a Bruker D8 Advance diffractometer equipped with a position sensitive detector Lynxeye in $\theta-2\theta$ geometry. Variable divergence slit and 2.3° Soller slit were used on the secondary side. The measurement was carried out in the range of $2\theta = 6-24°$ at a scan step of 0.018° at 40 kV and 40 mA utilizing Cu K$\alpha_{1,2}$ radiation (λ = 0.154018 nm). For the samples prepared on Si substrates, after background correction, the peak positions were calibrated using the substrate diffraction peak positions Si(400), which were measured additionally at the end of each run.

Photoluminescence Spectroscopy. Excitation and emission spectra were recorded with a resolution of ±1 nm using a photoluminescence spectrometer Horiba Jobin Yvon SpexFluorolog 3 (Horiba Jobin Yvon, Bensheim, Germany), equipped with a 450 W xenon lamp, double monochromators, Ulbricht sphere, and photo multiplier as the detector (90° angle between excitation source and detector). The determination of the absolute QY was performed as suggested by Friend.[59] The diffuse reflection of the sample was determined under excitation. Afterward, the emission was measured for the respective excitation wavelength. Integration over the reflected and emitted photons in the wavelength range of 390−720 nm using an Ulbricht sphere allowed for the absolute QY calculation. Standard corrections were used for the spectral power of the excitation source, the reflection behavior of the Ulbricht sphere, and the sensitivity of the detector. The QY was obtained for powder samples that were deposited in quartz glass tubes. The sample holder for determining the absolute QY in an Ulbricht sphere was constructed according to Friend.[59]

Scanning Electron Microscopy (SEM). The SEM measurements were performed on a ZEISS Gemini Leo 1530. The condition of a high vacuum was applied to all samples using 5 keV acceleration voltage.

Atomic Force Microscopy (AFM). The AFM topology measure ments were performed at room temperature on an Asylum Research MFP 3D BIO atomic force microscope in the alternating current mode (AC mode) with the scan rate of 0.4 Hz and 416 scan lines. A minimal number of modifications were performed in the raw data, which was modified by a masked flattening process.

Ground and excited state molecular calculations. All structures of the t F BDC ligand in the ground state were fully optimized using the hybrid B3LYP functional.[42−44] The S_1 and T_1 geometries were optimized using unrestricted time dependent density functional theory (TD DFT). Stationary points were characterized as the real minima on the potential energy surface by calculating the harmonic vibrational frequencies. The self consistent calculation (SCF) convergence threshold was set to 10^{-8} and "grid 3" option was used. For all atoms, triple ζ valence plus polarization (def2 TZVP)[54] atomic orbital basis sets were used. All simulations were performed within TURBOMOLE 7.4 DFT package.[60]

AUTHOR INFORMATION

Corresponding Author

Jaciara C. C. Santos − *Institute of Functional Interfaces (IFG), Karlsruhe Institute of Technology (KIT), 76344 Eggenstein Leopoldshafen, Germany;* orcid.org/0000 0003 2230 7903; Email: jaciara.santos3@kit.edu

Authors

Yohanes Pramudya − *Institute of Nanotechnology (INT), Karlsruhe Institute of Technology (KIT), 76344 Eggenstein Leopoldshafen, Germany;* orcid.org/0000 0002 0950 7655

Marjan Krstić − *Institute of Nanotechnology (INT), Karlsruhe Institute of Technology (KIT), 76344 Eggenstein Leopoldshafen, Germany*

Dong Hui Chen − *Institute of Functional Interfaces (IFG), Karlsruhe Institute of Technology (KIT), 76344 Eggenstein Leopoldshafen, Germany;* orcid.org/0000 0003 2561 2444

Beatrice Lilli Neumeier − *Institut für Anorganische Chemie, Karlsruhe Institute of Technology (KIT), 76131 Karlsruhe, Germany*

Claus Feldmann − *Institut für Anorganische Chemie, Karlsruhe Institute of Technology (KIT), 76131 Karlsruhe, Germany*

Wolfgang Wenzel − *Institute of Nanotechnology (INT), Karlsruhe Institute of Technology (KIT), 76344 Eggenstein Leopoldshafen, Germany*

Engelbert Redel − *Institute of Functional Interfaces (IFG), Karlsruhe Institute of Technology (KIT), 76344 Eggenstein Leopoldshafen, Germany*

Author Contributions

J.C.C.S., Y.P., and M.K. contributed equally. The manuscript was written through contributions of all authors. All authors have given approval to the final version of the manuscript.

Funding

Deutsche Forschungsgemeinschaft (DFG) within COORNET Priority Program, SPP 1928, Deutsche Forschungsgemein

schaft (DFG) under Germany's Excellence Strategy (2082/1 390761711), Chinese Scholarship Council (CSC), Baden Wuerttemberg Stiftung under Multi Skalen Modellierung von Materialien und Bauelementen für die Energieumwandlung und Energiespeicherung (MSMEE), and Deutsche For schungsgemeinschaft (DFG) WE 1863/29 1.

Notes

The authors declare no competing financial interest.

ACKNOWLEDGMENTS

Y.P. and W.W. acknowledge Baden Wuerttemberg Stiftung under Multi Skalen Modellierung von Materialien und Baue lementen für die Energieumwandlung und Energiespeicherung (MSMEE) and Deutsche Forschungsgemeinschaft (DFG, German Research Foundation) WE 1863/29 1. M.K. and W.W. acknowledge being funded by the DFG under Germany's Excellence Strategy, 2082/1 390761711. E.R. acknowledges financial support by the Deutsche Forschungs gemeinschaft (DFG) within the Priority Program COORNET Priority Program (SPP 1928). D. H.C. acknowledges the financial support of the Chinese Scholarship Council (CSC).

ABBREVIATIONS

Ln MOF, lanthanides metal−organic framework
SURMOFs, surface mounted metal−organic frameworks
LbL, layer by layer
QY, quantum yield
CN, coordination number
TD DFT, time dependent density functional theory
SBUs, secondary building units

REFERENCES

(1) Zhou, J.; Leaño, J. L.; Liu, Z.; Jin, D.; Wong, K. L.; Liu, R. S.; Bünzli, J. C. G. Impact of Lanthanide Nanomaterials on Photonic Devices and Smart Applications. *Small* **2018**, *14*, No. 1801882.

(2) Bünzli, J. C. G. Lanthanide Photonics: Shaping the Nanoworld. *Trends Chem.* **2019**, *1*, 751−762.

(3) Moghadam, P. Z.; Li, A.; Wiggin, S. B.; Tao, A.; Maloney, A. G. P.; Wood, P. A.; Ward, S. C.; Fairen Jimenez, D. Development of a Cambridge Structural Database Subset: A Collection of Metal−Organic Frameworks for Past, Present, and Future. *Chem. Mater.* **2017**, *29*, 2618−2625.

(4) Liu, J.; Wöll, C. Surface Supported Metal−Organic Framework Thin Films: Fabrication Methods, Applications, and Challenges. *Chem. Soc. Rev.* **2017**, *46*, 5730−5770.

(5) Cui, Y.; Yue, Y.; Qian, G.; Chen, B. Luminescent Functional Metal−Organic Frameworks. *Chem. Rev.* **2012**, *112*, 1126−1162.

(6) Allendorf, M. D.; Bauer, C. A.; Bhakta, R. K.; Houk, R. J. T. Luminescent Metal Organic Frameworks. *Chem. Soc. Rev.* **2009**, *38*, 1330−1352.

(7) Shekhah, O.; Wang, H.; Kowarik, S.; Schreiber, F.; Paulus, M.; Tolan, M.; Sternemann, C.; Evers, F.; Zacher, D.; Fischer, R. A.; Wöll, C. Step by Step Route for the Synthesis of Metal Organic Frame works. *J. Am. Chem. Soc.* **2007**, *129*, 15118−15119.

(8) Chen, D. H.; Haldar, R.; Neumeier, B. L.; Fu, Z. H.; Feldmann, C.; Wöll, C.; Redel, E. Tunable Emission in Heteroepitaxial Ln SURMOFs. *Adv. Funct. Mater.* **2019**, *29*, No. 1903086.

(9) Wang, Y.; Zhang, G.; Zhang, F.; Chu, T.; Yang, Y. A Novel Lanthanide MOF Thin Film: The Highly Performance Self Calibrating Luminescent Sensor for Detecting Formaldehyde as an Illegal Preservative in Aquatic Product. *Sens. Actuators, B* **2017**, *251*, 667−673.

(10) Liu, X.; Fu, W.; Bouwman, E. One Step Growth of Lanthanoid Metal Organic Framework (MOF) Films under Solvothermal Conditions for Temperature Sensing. *Chem. Commun.* **2016**, *52*, 6926−6929.

(11) Zhang, F.; Zhang, G.; Yao, H.; Wang, Y.; Chu, T.; Yang, Y. A Europium (III) Based Nano Flake MOF Film for Efficient Fluorescent Sensing of Picric Acid. *Microchim. Acta* **2017**, *184*, 1207−1213.

(12) Li, W. J.; Feng, J. F.; Lin, Z. J.; Yang, Y. Y. L.; Yang, Y. Y. L.; Wang, X. S.; Gao, S. Y.; Cao, R. Patterned Growth of Luminescent Metal Organic Framework Films: A Versatile Electrochemically Assisted Microwave Deposition Method. *Chem. Commun.* **2016**, *52*, 3951−3954.

(13) Guo, H.; Zhu, Y.; Qiu, S.; Lercher, J. A.; Zhang, H. Coordination Modulation Induced Synthesis of Nanoscale Eu1 XTbx Metal Organic Frameworks for Luminescent Thin Films. *Adv. Mater.* **2010**, *22*, 4190−4192.

(14) Feng, J. F.; Yang, X.; Gao, S. Y.; Shi, J.; Cao, R. Facile and Rapid Growth of Nanostructured Ln BTC Metal Organic Framework Films by Electrophoretic Deposition for Explosives Sensing in Gas and Cr 3+ Detection in Solution. *Langmuir* **2017**, *33*, 14238−14243.

(15) Feng, J. F.; Gao, S. Y.; Liu, T. F.; Shi, J.; Cao, R. Preparation of Dual Emitting Ln@UiO 66 Hybrid Films via Electrophoretic Depo sition for Ratiometric Temperature Sensing. *ACS Appl. Mater. Interfaces* **2018**, *10*, 6014−6023.

(16) Meyer, L. V.; Schönfeld, F.; Buschbaum, K. M. Lanthanide Based Tuning of Luminescence in MOFs and Dense Frameworks − from Mono and Multimetal Systems to Sensors and Films. *Chem. Commun.* **2014**, *50*, 8093−8108.

(17) Sabbatini, N.; Guardigli, M.; Lehn, J. M. Luminescent Lanthanide Complexes as Photochemical Supramolecular Devices. *Coord. Chem. Rev.* **1993**, *123*, 201−228.

(18) Freidzon, A. Y.; Scherbinin, A. V.; Bagaturyants, A. A.; Alfimov, M. V. Ab Initio Study of Phosphorescent Emitters Based on Rare Earth Complexes with Organic Ligands for Organic Electro luminescent Devices. *J. Phys. Chem. A* **2011**, *115*, 4565−4573.

(19) Romanova, K. A.; Freidzon, A. Y.; Bagaturyants, A. A.; Galyametdinov, Y. G. Ab Initio Study of Energy Transfer Pathways in Dinuclear Lanthanide Complex of Europium(III) and Terbium(III) Ions. *J. Phys. Chem. A* **2014**, *118*, 11244−11252.

(20) Kovalenko, A. D.; Bushmarinov, I. S.; Burlov, A. S.; Lepnev, L. S.; Ilina, E. G.; Utochnikova, V. V. The Peculiarities of Complex Formation and Energy Transfer Processes in Lanthanide Complexes with 2 (Tosylamino) Benzylidene N Benzoylhydrazone. *Dalton Trans.* **2018**, *47*, 4524−4533.

(21) Guo, X.; Zhu, G.; Sun, F.; Li, Z.; Zhao, X.; Li, X.; Wang, H.; Qiu, S. Synthesis, Structure, and Luminescent Properties of Microporous Lanthanide Metal−Organic Frameworks with Inorganic Rod Shaped Building Units. *Inorg. Chem.* **2006**, *45*, 2581−2587.

(22) Seidel, C.; Lorbeer, C.; Cybińska, J.; Mudring, A. V.; Ruschewitz, U. Lanthanide Coordination Polymers with Tetrafluor oterephthalate as a Bridging Ligand: Thermal and Optical Properties. *Inorg. Chem.* **2012**, *51*, 4679−4688.

(23) Le Natur, F.; Calvez, G.; Freslon, S.; Daiguebonne, C.; Bernot, K.; Guillou, O. Extending the Lanthanide Terephthalate System: Isolation of an Unprecedented Tb(III) Based Coordination Polymer with High Potential Porosity and Luminescence Properties. *J. Mol. Struct.* **2015**, *1086*, 34−42.

(24) Sobieray, M.; Gode, J.; Seidel, C.; Poß, M.; Feldmann, C.; Ruschewitz, U. Bright Luminescence in Lanthanide Coordination Polymers with Tetrafluoroterephthalate as a Bridging Ligand. *Dalton Trans.* **2015**, *44*, 6249−6259.

(25) Chen, B.; Yang, Y.; Zapata, F.; Qian, G.; Luo, Y.; Zhang, J.; Lobkovsky, E. Enhanced Near Infrared−Luminescence in an Erbium Tetrafluoroterephthalate Framework. *Inorg. Chem.* **2006**, *45*, 8882−8886.

(26) Smith, J. A.; Singh Wilmot, M. A.; Carter, K. P.; Cahill, C. L.; Ridenour, J. A. Lanthanide 2,3,5,6 Tetrabromoterephthalic Acid Metal−Organic Frameworks: Evolution of Halogen···Halogen Inter actions across the Lanthanide Series and Their Potential as Selective

Bifunctional Sensors for the Detection of Fe^{3+}, Cu^{2+}. *Cryst. Growth Des.* **2019**, *19*, 305−319.
(27) Chen, S. C.; Dai, A. Q.; Huang, K. L.; Zhang, Z. H.; Cui, A. J.; He, M. Y.; Chen, Q. Assembly of 1D, 2D and 3D Lanthanum(Iii) Coordination Polymers with Perchlorinated Benzenedicarboxylates: Positional Isomeric Effect, Structural Transformation and Ring Opening Polymerisation of Glycolide. *Dalton Trans.* **2016**, *45*, 3577−3589.
(28) Müller Buschbaum, K. Group 3 Elements and Lanthanide Metals. In *The Chemistry of Metal Organic Frameworks: Synthesis, Characterization, and Applications*; Wiley VCH Verlag GmbH & Co. KGaA: Weinheim, Germany, 2016; pp 231−270.
(29) Xia, J.; Zhao, B.; Wang, H. S.; Shi, W.; Ma, Y.; Song, H. B.; Cheng, P.; Liao, D. Z.; Yan, S. P. Two and Three Dimensional Lanthanide Complexes: Synthesis, Crystal Structures, and Properties. *Inorg. Chem.* **2007**, *46*, 3450−3458.
(30) Pagis, C.; Ferbinteanu, M.; Rothenberg, G.; Tanase, S. Lanthanide Based Metal Organic Frameworks: Synthetic Strategies and Catalytic Applications. *ACS Catal.* **2016**, *6*, 6063−6072.
(31) Choppin, G. R.; Wang, Z. M. Correlation between Ligand Coordination Number and the Shift of the 7F0−5D0 Transition Frequency in Europium(III) Complexes. *Inorg. Chem.* **1997**, *36*, 249−252.
(32) Reineke, T. M.; Eddaoudi, M.; Fehr, M.; Kelley, D.; Yaghi, O. M. From Condensed Lanthanide Coordination Solids to Microporous Frameworks Having Accessible Metal Sites. *J. Am. Chem. Soc.* **1999**, *121*, 1651−1657.
(33) Pan, L.; Zheng, N.; Wu, Y.; Han, S.; Yang, R.; Huang, X.; Li, J. Synthesis, Characterization and Structural Transformation of a Condensed Rare Earth Metal Coordination Polymer. *Inorg. Chem.* **2001**, *40*, 828−830.
(34) Xie, S. L.; Xie, B. Q.; Tang, X. Y.; Wang, N.; Yue, S. T. Hydrothermal Synthesis, Structures and Thermal Stability of Two Novel Lanthanide Complexes: $[Er_4(Tp)_6(H_2O)_6]$, $[Lu(Tp)_{1.5}(H_2O)_3]$. *Z. Anorg. Allg. Chem.* **2008**, *634*, 842−844.
(35) Decadt, R.; Van Hecke, K.; Depla, D.; Leus, K.; Weinberger, D.; Van Driessche, I.; Van Der Voort, P.; Van Deun, R. Synthesis, Crystal Structures, and Luminescence Properties of Carboxylate Based Rare Earth Coordination Polymers. *Inorg. Chem.* **2012**, *51*, 11623−11634.
(36) Yi, P.; Huang, H.; Peng, Y.; Liu, D.; Zhong, C. A Series of Europium Based Metal Organic Frameworks with Tuned Intrinsic Luminescence Properties and Detection Capacities. *RSC Adv.* **2016**, *6*, 111934−111941.
(37) Wei, L.; Ye, Y.; Zhang, R. Synthesis, Crystal Structure and Fluorescence Properties of Nd3+ Complex with Tetrabromotereph thalic Acid. *J. Mol. Struct.* **2014**, *1058*, 51−55.
(38) MacNeill, C. M.; Day, C. S.; Marts, A.; Lachgar, A.; Noftle, R. E. Synthesis, Crystal Structure and Properties of Novel Isostructural Two Dimensional Lanthanide Based Coordination Polymers with 2,3,5,6 Tetrafluoro 1,4 Benzenedicarboxylic Acid. *Inorg. Chim. Acta* **2011**, *365*, 196−203.
(39) Vaitsis, C.; Sourkouni, G.; Argirusis, C. Metal Organic Frameworks (MOFs) and Ultrasound: A Review. *Ultrason. Sonochem.* **2019**, *52*, 106−119.
(40) Khan, N. A.; Haque, M. M.; Jhung, S. H. Accelerated Syntheses of Porous Isostructural Lanthanide Benzenetricarboxylates (Ln BTC) under Ultrasound at Room Temperature. *Eur. J. Inorg. Chem.* **2010**, *2010*, 4975−4981.
(41) Yang, D.; Tian, Y.; Xu, W.; Cao, X.; Zheng, S.; Ju, Q.; Huang, W.; Fang, Z. A Series of Lanthanide Based Metal−Organic Frame works: Synthesis, Structures, and Multicolor Tuning of Single Component. *Inorg. Chem.* **2017**, *56*, 2345−2353.
(42) Tobita, S.; Arakawa, M.; Tanaka, I. The Paramagnetic Metal Effect on the Ligand Localized S1.Apprx..Fwdarw. T1 Intersystem Crossing in the Rare Earth Metal Complexes with Methyl Salicylate. *J. Phys. Chem. A* **1985**, *89*, 5649−5654.
(43) Faustino, W. M.; Malta, O. L.; Teotonio, E. E. S.; Brito, H. F.; Simas, A. M.; de Sá, G. F. Photoluminescence of Europium(III) Dithiocarbamate Complexes: Electronic Structure, Charge Transfer and Energy Transfer. *J. Phys. Chem. A* **2006**, *110*, 2510−2516.
(44) de Andrade, A. V. M.; Longo, R. L.; Simas, A. M.; de Sá, G. F. Theoretical Model for the Prediction of Electronic Spectra of Lanthanide Complexes. *J. Chem. Soc., Faraday Trans.* **1996**, *92*, 1835−1839.
(45) Ermolaev, V.; Sveshnikova, E.; Bodunov, E. Inductive Resonant Mechanism of Nonradiative Transitions in Ions and Molecules in Condensed Phase. *Phys. Usp.* **1996**, *39*, 261−282.
(46) Sato, S.; Wada, M. Relations between Intramolecular Energy Transfer Efficiencies and Triplet State Energies in Rare Earth β Diketone Chelates. *Bull. Chem. Soc. Jpn.* **1970**, *43*, 1955−1962.
(47) Latva, M.; Takalo, H.; Mukkala, V. M.; Matachescu, C.; Rodríguez Ubis, J. C.; Kankare, J. Correlation between the Lowest Triplet State Energy Level of the Ligand and Lanthanide(III) Luminescence Quantum Yield. *J. Lumin.* **1997**, *75*, 149−169.
(48) Mikhalyova, E. A.; Smola, S. S.; Garvilenko, K. S.; Dotsenko, V. P.; Eremenko, I. L.; Pavlishchuk, V. V. Metal Centered Photo luminescence of Eu3+ and Tb3+ Coordination Polymers with Dianions of Camphoric and Tetrafluoroterephthalic Acids. *Theor. Exp. Chem.* **2015**, *51*, 30−36.
(49) Binnemans, K. Lanthanide Based Luminescent Hybrid Materials. *Chem. Rev.* **2009**, *109*, 4283−4374.
(50) White, K. A.; Chengelis, D. A.; Gogick, K. A.; Stehman, J.; Rosi, N. L.; Petoud, S. Near Infrared Luminescent Lanthanide MOF Barcodes. *J. Am. Chem. Soc.* **2009**, *131*, 18069−18071.
(51) Liu, J.; Yee, K. K.; Lo, K. K. W.; Zhang, K. Y.; To, W. P.; Che, C. M.; Xu, Z. Selective Ag(I) Binding, H2S Sensing, and White Light Emission from an Easy to Make Porous Conjugated Polymer. *J. Am. Chem. Soc.* **2014**, *136*, 2818−2824.
(52) Dutra, J. D. L.; Bispo, T. D.; Freire, R. O. LUMPAC Lanthanide Luminescence Software: Efficient and User Friendly. *J. Comput. Chem.* **2014**, *35*, 772−775.
(53) Malta, O. L. Mechanisms of Non Radiative Energy Transfer Involving Lanthanide Ions Revisited. *J. Non Cryst. Solids* **2008**, *354*, 4770−4776.
(54) Weigend, F.; Ahlrichs, R. Balanced Basis Sets of Split Valence, Triple Zeta Valence and Quadruple Zeta Valence Quality for H to Rn: Design and Assessment of Accuracy. *Phys. Chem. Chem. Phys.* **2005**, *7*, 3297.
(55) Neese, F. The ORCA Program System. *Wiley Interdiscip. Rev. Comput. Mol. Sci.* **2012**, *2*, 73−78.
(56) Judd, B. R. Optical Absorption Intensities of Rare Earth Ions. *Phys. Rev.* **1962**, *127*, No. 750.
(57) Ofelt, G. S. Intensities of Crystal Spectra of Rare Earth Ions. *J. Chem. Phys.* **1962**, *37*, 511−520.
(58) Malta, O. L.; Brito, H. F.; Menezes, J. F. S.; Gonçalves e Silva, F. R.; de Mello Donegá, C.; Alves, S. Experimental and Theoretical Emission Quantum Yield in the Compound Eu (Thenoyltrifluoroacetonate)3.2(Dibenzyl Sulfoxide). *Chem. Phys. Lett.* **1998**, *282*, 233−238.
(59) de Mello, J. C.; Wittmann, H. F.; Friend, R. H. An Improved Experimental Determination of External Photoluminescence Quan tum Efficiency. *Adv. Mater.* **1997**, *9*, 230−232.
(60) Balasubramani, S. G.; Chen, G. P.; Coriani, S.; Diedenhofen, M.; Frank, M. S.; Franzke, Y. J.; Furche, F.; Grotjahn, R.; Harding, M. E.; Hättig, C.; Hellweg, A.; Helmich Paris, B.; Holzer, C.; Huniar, U.; Kaupp, M.; Marefat Khah, A.; Karbalaei Khani, S.; Müller, T.; Mack, F.; Nguyen, B. D.; Parker, S. M.; Perlt, E.; Rappoport, D.; Reiter, K.; Roy, S.; Rückert, M.; Schmitz, G.; Sierka, M.; Tapavicza, E.; Tew, D. P.; van Wüllen, C.; Voora, V. K.; Weigend, F.; Wodyński, A.; Yu, J. M. TURBOMOLE: Modular Program Suite for Ab Initio Quantum Chemical and Condensed Matter Simulations. *J. Chem. Phys.* **2020**, *152*, No. 184107.